(*R*)-PFI-2 is a potent and selective inhibitor of SETD7 methyltransferase activity in cells

Dalia Barsyte-Lovejoy[a,1,2], Fengling Li[a,1], Menno J. Oudhoff[b,1], John H. Tatlock[c,1], Aiping Dong[a], Hong Zeng[a], Hong Wu[a], Spencer A. Freeman[d], Matthieu Schapira[a,e], Guillermo A. Senisterra[a], Ekaterina Kuznetsova[a], Richard Marcellus[f], Abdellah Allali-Hassani[a], Steven Kennedy[a], Jean-Philippe Lambert[g], Amber L. Couzens[g], Ahmed Aman[f], Anne-Claude Gingras[g,h], Rima Al-Awar[e,f], Paul V. Fish[i,3], Brian S. Gerstenberger[j], Lee Roberts[k], Caroline L. Benn[l], Rachel L. Grimley[l], Mitchell J. S. Braam[b], Fabio M. V. Rossi[b,m], Marius Sudol[n], Peter J. Brown[a], Mark E. Bunnage[k], Dafydd R. Owen[k], Colby Zaph[b,o], Masoud Vedadi[a,e,2], and Cheryl H. Arrowsmith[a,p,2]

[a]Structural Genomics Consortium, University of Toronto, Toronto, ON, Canada M5G 1L7; [b]Biomedical Research Centre, University of British Columbia, Vancouver, BC, Canada V6T1Z3; [c]Worldwide Medicinal Chemistry, Pfizer Worldwide Research and Development, San Diego, CA 92121; [d]Department of Microbiology and Immunology, University of British Columbia, Vancouver, BC, Canada V6T1Z3; [e]Department of Pharmacology and Toxicology, University of Toronto, Toronto, ON, Canada M5S 1A8; [f]Drug Discovery Program, Ontario Institute for Cancer Research, Toronto, ON, Canada M5G 0A3; [g]Centre for Systems Biology, Lunenfeld-Tanenbaum Research Institute, Toronto, ON, Canada M5G 1X5; [h]Department of Molecular Genetics, University of Toronto, Toronto, ON, Canada M5S 1A8; [i]Worldwide Medicinal Chemistry, Pfizer Worldwide Research and Development, Sandwich, Kent CT13 9NJ, United Kingdom; [j]Worldwide Medicinal Chemistry, Pfizer Worldwide Research and Development, Groton, CT 06340; [k]Worldwide Medicinal Chemistry, Pfizer Worldwide Research and Development, Cambridge, MA 02139; [l]Neusentis Research Unit, Pfizer Worldwide Research and Development, Cambridge CB21 6GS, United Kingdom; [m]Department of Medical Genetics, University of British Columbia, Vancouver, BC, Canada V6T1Z3; [n]Weis Center for Research, Geisinger Clinic, Danville, PA 17821; [o]Department of Pathology and Laboratory Medicine, University of British Columbia, Vancouver, BC, Canada V6T1Z3; and [p]Princess Margaret Cancer Centre and Department of Medical Biophysics, University of Toronto, ON, Canada M5G 1L7

Edited by Robert J. Fletterick, University of California, San Francisco School of Medicine, San Francisco, CA, and approved July 22, 2014 (received for review April 22, 2014)

SET domain containing (lysine methyltransferase) 7 (SETD7) is implicated in multiple signaling and disease related pathways with a broad diversity of reported substrates. Here, we report the discovery of (*R*)-PFI-2—a first-in-class, potent (K_i^{app} = 0.33 nM), selective, and cell-active inhibitor of the methyltransferase activity of human SETD7—and its 500-fold less active enantiomer, (*S*)-PFI-2. (*R*)-PFI-2 exhibits an unusual cofactor-dependent and substrate-competitive inhibitory mechanism by occupying the substrate peptide binding groove of SETD7, including the catalytic lysine-binding channel, and by making direct contact with the donor methyl group of the cofactor, *S*-adenosylmethionine. Chemoproteomics experiments using a biotinylated derivative of (*R*)-PFI-2 demonstrated dose-dependent competition for binding to endogenous SETD7 in MCF7 cells pretreated with (*R*)-PFI-2. In murine embryonic fibroblasts, (*R*)-PFI-2 treatment phenocopied the effects of *Setd7* deficiency on Hippo pathway signaling, via modulation of the transcriptional coactivator Yes-associated protein (YAP) and regulation of YAP target genes. In confluent MCF7 cells, (*R*)-PFI-2 rapidly altered YAP localization, suggesting continuous and dynamic regulation of YAP by the methyltransferase activity of SETD7. These data establish (*R*)-PFI-2 and related compounds as a valuable tool-kit for the study of the diverse roles of SETD7 in cells and further validate protein methyltransferases as a druggable target class.

epigenetics | chemical biology | chemical probe

Protein methyltransferases play diverse roles in the epigenetic regulation of gene transcription, silencing, chromatin structure establishment, maintenance, DNA repair, and replication. SET domain containing (lysine methyltransferase) 7 (SETD7) (SET9; SET7/9, KMT7) was one of the first protein lysine methyltransferases to be discovered and was originally characterized as a monomethyltransferase of lysine 4 on histone H3 (H3K4me1) (1, 2). Subsequently, SETD7 has been shown to have a very broad target specificity in vitro, including transcriptional regulators such as TAF10, p53, ER, p65, STAT3, Rb, Mypt, Tat, and Foxo3 (3–16). SETD7 is also reported to regulate DNA methyltransferase 1 (DNMT1) in a brain-specific manner (14) and functionally interacts with Pdx1 in pancreatic β cells (6). The diverse nature of its substrates has implicated SETD7 in multiple molecular pathways involved in cancer, metabolism, and inflammation. Despite these diverse substrates and molecular pathways, mice with a genetic deletion of *Setd7* have no obvious developmental deficiencies and do not prematurely develop cancer (17, 18). Thus, the exact functional role of SETD7 in normal or disease biology is still an open question (10).

SETD7 contains a SET [Su(var)3–9 and Enhancer of Zeste-Trithorax] domain that is conserved among many *S*-adenosylmethionine (SAM)-dependent protein lysine methyltransferases (PKMTs) (19). SETD7 has robust monomethyltransferase activity

Significance

Protein methyltransferases constitute an emerging but under-characterized class of therapeutic targets with diverse roles in normal human biology and disease. Small-molecule "chemical probes" can be powerful tools for the functional characterization of such enzymes, and here we report the discovery of (*R*)-PFI-2—a first-in-class, potent, highly selective, and cell-active inhibitor of the methyltransferase activity of SETD7 [SET domain containing (lysine methyltransferase) 7]—and two related compounds for control and chemoproteomics studies. We used these compounds to characterize the role of SETD7 in signaling, in the Hippo pathway, that controls cell growth and organ size. Our work establishes a chemical biology tool kit for the study of the diverse roles of SETD7 in cells and further validates protein methyltransferases as a druggable target class.

Author contributions: D.B.-L., M.J.O., J.H.T., M. Schapira, J.-P.L., A.L.C., A.-C.G., R.A.-A., P.V.F., B.S.G., L.R., C.L.B., R.L.G., P.J.B., M.E.B., D.R.O., C.Z., M.V., and C.H.A. designed research; D.B.-L., F.L., M.J.O., A.D., H.Z., H.W., S.A.F., G.A.S., E.K., R.M., A.A.-H., S.K., J.-P.L., A.L.C., A.A., and R.L.G. performed research; M.J.S.B., F.M.V.R., and M. Sudol contributed new reagents/analytic tools; D.B.-L., F.L., M.J.O., J.H.T., A.D., H.W., M. Schapira, E.K., R.M., A.A.-H., S.K., J.-P.L., A.L.C., A.A., R.A.-A., P.V.F., B.S.G., L.R., C.L.B., R.L.G., D.R.O., C.Z., M.V., and C.H.A. analyzed data; and D.B.-L., M.J.O., J.H.T., M. Schapira, A.-C.G., P.J.B., M.E.B., D.R.O., C.Z., M.V., and C.H.A. wrote the paper.

The authors declare no conflict of interest.

This article is a PNAS Direct Submission.

Data deposition: The atomic coordinates and structure factors have been deposited in the Protein Data Bank, www.pdb.org (PDB ID code 4JLG).

[1]D.B.-L., F.L., M.J.O., and J.H.T. contributed equally to this work.

[2]To whom correspondence may be addressed. Email: carrow@uhnres.utoronto.ca, m.vedadi@utoronto.ca, or d.barsyte@utoronto.ca.

[3]Present address: University College London School of Pharmacy, London WC1N 1AX, United Kingdom.

This article contains supporting information online at www.pnas.org/lookup/suppl/doi:10.1073/pnas.1407358111/-/DCSupplemental.

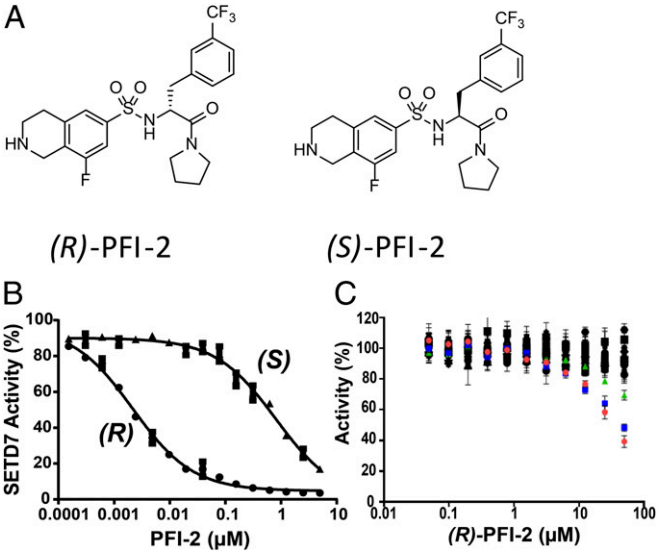

Fig. 1. (*R*)-PFI-2 is a potent inhibitor of SETD7. (*A*) Chemical structures of SETD7 inhibitors (*R*)-PFI-2 and its less-active enantiomer (*S*)-PFI-2. (*B*) The effect of (*R*)-PFI-2 (●) and (*S*)-PFI-2 (▲) on methyltransferase activity of SETD7. Compounds inhibited SETD7 activity with IC_{50} values of 2.0 ± 0.2 nM (Hill slope, 0.8) and 1.0 ± 0.1 μM (Hill slope: 0.7), respectively. All experiments were performed in quadruplicate. (*C*) Effect of (*R*)-PFI-2 on activity of 18 different protein methyltransferases [(red filled circle) G9a, (blue filled square) EZH2, (green filled triangle) EHMT1, SUV39H2, EZH1, SUV420H1, SUV420H2, SETD8, SETD2, PRMT1, PRMT3, PRMT5, PRMT8, SETDB1, MLL1, DOT1L, WHSC1, and SMYD2] and DNMT1 was assessed using as high as 50 μM (*R*)-PFI-2. Experiments were performed in triplicate.

on H3K4 N-terminal peptides in vitro, but little or no enzymatic activity when nucleosomal H3 is used as the substrate (1, 2). Furthermore, knockdown or depletion of SETD7 does not affect the global cellular levels of the H3K4me1 mark (17, 18), raising the question of the physiological context of H3 as a substrate (10). Increasing evidence supports a role for SETD7 in methylation of diverse nonhistone proteins, especially transcription factors and chromatin regulatory complexes, leading to changes in gene-expression programs, some of which were shown to involve loci-specific H3K4 monomethylation (reviewed in ref. 10). Peptide array studies in vitro have identified a consensus SETD7 substrate sequence found in previously reported SETD7 substrates as well as novel targets (7). Nevertheless, the functional significance of most of these targets is largely unexplored.

In addition to its broad substrate specificity, SETD7 also has unique features that distinguish it from most other PKMTs. First, SETD7 has neither canonical nuclear localization signals nor nuclear export signals and has been reported to localize in both the cytoplasm and the nucleus (20, 21). Thus, nuclear localization of SETD7 may be regulated, at least in part, via interaction with other cellular factors. For example, SETD7 is recruited to the promoters of target genes by interacting with transcription factors such as NFκB (20). Secondly, SETD7 is the only methyltransferase that contains membrane occupation and recognition nexus (MORN) repeats that are found in proteins linking the membrane to the cytoskeleton (22). This observation suggests a potential cytoplasmic role for SETD7. Given the multitude of methylation and interaction targets and paucity of distinct SETD7-associated phenotypes identified to date, it is likely that SETD7 function may be modulatory, subtle, and highly dependent on the cell type and/or physiological conditions being studied.

Recently, the identification of chemical probes (23, 24)—potent, selective, cell-active small molecules—for protein methyltransferases such as G9a, DOT1L, and EZH2 has greatly enabled the investigation of the functional biology of these enzymes, as well as the exploration of their potential as therapeutic targets (25). Here, we describe the discovery of (*R*)-PFI-2, a potent and selective inhibitor of SETD7, and its use in modulation of the Hippo pathway by SETD7 inhibition. Thus, (*R*)-PFI-2, together with its 500-fold less-active enantiomer (*S*)-PFI-2 and a biotinylated derivative of (*R*)-PFI-2, provides a chemical probe tool kit to interrogate the biology of SETD7.

Results

(*R*)-PFI-2 Is a Potent, Selective Inhibitor of SETD7 Methyltransferase Activity. The discovery of (*R*)-PFI-2 (Fig. 1*A*) was initiated with a high-throughput screen (HTS) of a 150,000-compound subset of Pfizer's full HTS collection in an in vitro enzymatic assay of recombinant SETD7. After several rounds of structure-guided molecular design, including optimization of cell permeability, the inhibition of SETD7 in vitro catalytic activity was improved >100-fold compared with the initial HTS hit (IC_{50} of 2.1 μM), resulting in (*R*)-PFI-2 (synthesis provided in *SI Appendix*).

A robust radioactivity-based assay was used to determine kinetic parameters for methyltransferase activity of SETD7 and to characterize inhibitors (Table 1 and *SI Appendix*, Fig. S1). (*R*)-PFI-2 inhibited the methyltransferase activity of human SETD7 with an IC_{50} value of 2.0 ± 0.2 nM whereas its enantiomer, (*S*)-PFI-2, was 500-fold less active (IC_{50} value of 1.0 ± 0.1 μM), making the latter an excellent compound for use as a negative control (24) in chemical biology experiments (Table 1 and Fig. 1*B*). Measurement of the fractional velocities as a function of (*R*)-PFI-2 concentration yielded a Morrison K_i^{app} (26, 27) value of 0.33 ± 0.04 nM, confirming that (*R*)-PFI-2 potently inhibits SETD7 in vitro (*SI Appendix*, Fig. S1*D*). (*R*)-PFI-2 is highly selective (>1,000-fold) for SETD7, over a panel of 18 other human protein methyltransferases and DNMT1, and was shown to be inactive against 134 additional ion channel, GPCR, and enzyme targets (<35% inhibition at 10 μM) (Fig. 1*C* and *SI Appendix*, Table S1).

(*R*)-PFI-2 Binds in the Substrate-Binding Pocket. To better understand the inhibitory mechanism, we solved the X-ray crystal structure of the human SETD7 catalytic domain bound to (*R*)-PFI-2 at 1.9-Å resolution, revealing that the inhibitor occupies part of the substrate peptide-binding groove of the enzyme extending deep into the lysine-binding active site (Fig. 2 and *SI Appendix*, Fig. S2 and Table S2). There are several noteworthy features of this interaction. First, an intramolecular pi-stacking interaction between the phenyl group of the inhibitor's tetrahydroisoquinoline core and the trifluoromethylated phenylalanine substructure leads to a compact conformation of the protein-bound inhibitor. Second, (*R*)-PFI-2 efficiently occupies the portion of the peptide-binding groove that is normally occupied by the target lysine residue and the peptide backbone of the preceding two residues of the substrate peptide (Fig. 2 *A* and *C*–*E*). These two residues (-1 and -2 relative to substrate Lys) have been shown to be the most important residues for substrate binding by SETD7 (7), suggesting that (*R*)-PFI-2 will be effective at inhibiting

Table 1. Enzymatic characterization of wild-type SETD7 and mutants

Protein	K_m^{app}, μM		k_{cat}, h^{-1}	(*R*)-PFI-2 IC_{50}, nM*
	Peptide	SAM		
Wild-type	1.1 ± 0.1	0.3 ± 0.1	48 ± 2	2.0 ± 0.2
H252W	1.8 ± 0.2	0.5 ± 0.1	37 ± 4	2,630 ± 200
D256A	1.9 ± 0.1	0.4 ± 0.1	7 ± 1	1,200 ± 90
V274E	3.1 ± 0.2	0.7 ± 0.2	3 ± 0.5	10,770 ± 2,000

*Methods are described in *SI Appendix*. All experiments were performed in triplicate, and values are presented as mean values ± SD.

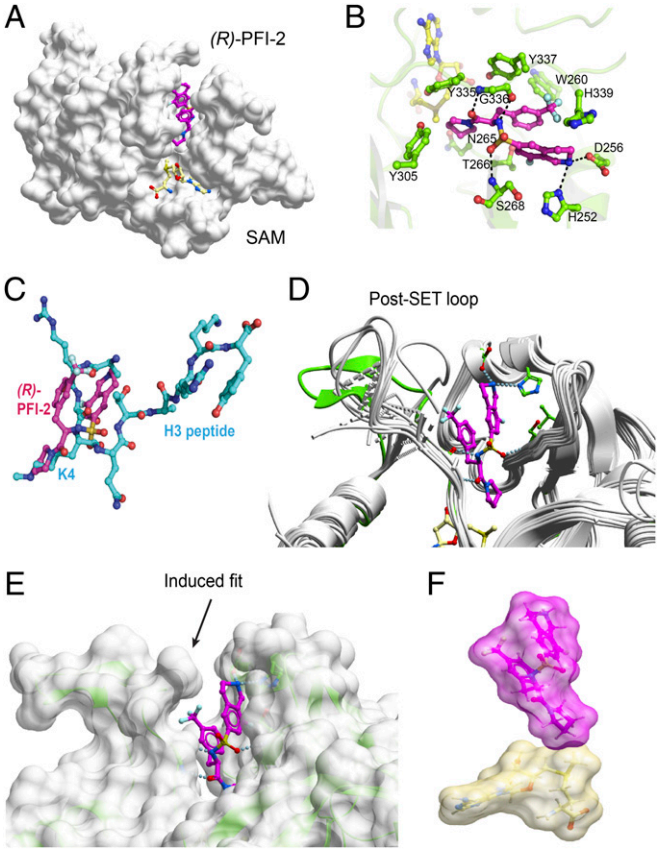

Fig. 2. Structure and binding mode of (*R*)-PFI-2. (*A*) Molecular graphics of the 1.9-Å crystal structure of (*R*)-PFI-2 (magenta) bound within the substrate peptide-binding groove of human SETD7 (surface representation in gray). The cofactor, SAM, is in yellow. (*B*) Detailed interactions between SETD7 (green) and (*R*)-PFI-2 (magenta). Hydrogen bonds are shown as dashed lines. (*C*) Superimposition of (*R*)-PFI-2 with the SETD7-bound conformation of a substrate histone peptide (PDB ID code 1O9S) (28), showing partial occupation of the peptide-binding site by (*R*)-PFI-2. (*D*) Superimposition of (*R*)-PFI-2–bound SETD7 (green) with all 23 SETD7 structures in complex with cofactor (or cofactor mimic, sinefungin) available from the PDB (gray), showing the conformational variability of the post-SET loop. SETD7 residues that form H-bonds to (*R*)-PFI-2 are shown in green and are located in the less conformationally variable region of the protein. (*E*) Surface representation of (*R*)-PFI-2–bound SETD7 highlighting an induced conformation of the post-SET loop (green) that is not seen in any of the other SETD7 structures. (*F*) Molecular surface representation of SAM (yellow) and (*R*)-PFI-2 (purple), highlighting hydrophobic interactions between the methyl group of SAM and the pyrrolidine moiety of the inhibitor.

the wide variety of SETD7 substrates. The pyrrolidine amide occupies the lysine-binding channel and makes direct hydrophobic interactions with the departing methyl group of SAM (Fig. 2 *B* and *F*), further preventing productive interaction of SETD7 with lysine substrates. Third, binding of (*R*)-PFI-2 induces a unique conformation of the post-SET loop (residues 336–349), which normally forms one "wall" of the peptide-binding groove of the enzyme. In previous crystal structures of SETD7, the conformation of this post-SET loop is highly variable and often lacks electron density (Fig. 2*D*). However, in the (*R*)-PFI-2–bound structure, the post-SET loop has an optimized shape complementarity and forms hydrophobic interactions with the trifluoromethyl moiety of (*R*)-PFI-2 (Fig. 2 *D* and *E*). Fourth, a network of hydrogen bonds with G336 at the base of the post-SET loop, and with the opposite wall of the substrate binding groove (S268, H252, and D256 in the structurally invariable I-SET subdomain), anchor the ligand within the peptide-binding site.

The importance of these residues for inhibitory activity by (*R*)-PFI-2 was verified by site-directed mutagenesis (Table 1). First, H252 contributes an important hydrogen bond to (*R*)-PFI-2 binding (Fig. 2*B*) but does not interact with the H3 peptide substrate (PDB ID code 1O9S) (28). Mutation of H252 to tryptophan resulted in an enzyme that was as active as the wild-type protein for the H3(1–25) substrate, but for which the inhibitory effect of (*R*)-PFI-2 was reduced more than 1,000-fold (Table 1), confirming that this interaction makes important contributions to the mode of inhibition by (*R*)-PFI-2. We also evaluated two mutants of residues that are involved in both (*R*)-PFI-2 and peptide binding, D256A and V274E (Table 1). Although these mutants had no significant change in K_m values for SAM and peptide, both had much lower activity (k_{cat} values of 7 ± 1 and 3 ± 0.5 h^{-1}, respectively). These two mutations also displayed a dramatic increase in IC_{50} values for (*R*)-PFI-2, consistent with the mode of binding observed in the crystal structure. These data clearly indicate that (*R*)-PFI-2 binds within the peptide-binding site with unique interactions that contribute to its high potency, while also interacting with residues that contribute to peptide binding and enzymatic activity. Finally, our structural data also predict that (*S*)-PFI-2 is unable to form the full set of interactions observed for (*R*)-PFI-2 (Fig. 2*B*), explaining its reduced inhibitory activity.

(*R*)-PFI-2 Is a SAM-Dependent Inhibitor. Our structural data indicate that (*R*)-PFI-2 (*i*) occupies the peptide binding groove, (*ii*) induces conformational alterations in the post-SET loop, and (*iii*) makes direct contact with SAM, suggesting a peptide-competitive mode of inhibition that may also be dependent on SAM binding. Moreover, it is well-known that SAM binding to SET domain methyltransferases has an important role in folding and stabilizing the post-SET loop (19), and SETD7 has been reported to have an ordered binding mechanism in which SAM first binds the enzyme, followed by peptide binding (29). Together these observations further hint at a structural interdependence between SAM binding and binding of ligands that occupy the peptide-binding groove formed by the post-SET loop.

To investigate in more detail the binding properties of (*R*)-PFI-2, we next performed surface plasmon resonance (SPR) experiments, confirming that (*R*)-PFI-2 binds to SETD7 only in the presence of SAM (Fig. 3*A*). Fast on and off rates were observed for SAM binding alone (Fig. 3*A*, green trace) whereas (*R*)-PFI-2 alone exhibited no binding to SETD7 (Fig. 3*A*, red trace). Inclusion of 20 μM SAM in (*R*)-PFI-2 binding injections (but no SAM in the flow/wash buffer) resulted in binding and dissociation curves reflecting both SAM and (*R*)-PFI-2 contributions (Fig. 3*A*, blue trace). In the presence of constant 20 μM SAM in the flow and wash buffer, (*R*)-PFI-2 binds with an on rate of 1.4 ± 0.16 × 10^6 $M^{-1}{\cdot}s^{-1}$ and off rate of 0.0058 ± 0.0009 s^{-1} yielding a K_D value of 4.2 ± 0.2 nM (*SI Appendix*, Fig. S3). Taken together, these data are consistent with a significant role for SAM in the binding of (*R*)-PFI-2 to SETD7, as observed in our crystal structure, and suggest that the enzyme-inhibitory kinetics are likely defined by codependence on both cofactor and substrate concentrations.

Finally, to further investigate the mode of action of (*R*)-PFI-2, we determined the IC_{50} values at varying SAM and peptide concentrations (30) (Fig. 3 *B* and *C*). A decrease in IC_{50} values at fixed peptide concentration (5 μM) and increasing SAM concentration indicated an uncompetitive mode of inhibition with respect to SAM (Fig. 3*B*), consistent with our SPR data indicating that (*R*)-PFI-2 binds to SETD7 only in the presence of SAM (Fig. 3*A*). At a saturating concentration of SAM (2 μM) and increasing concentration of peptide, (*R*)-PFI-2 displayed an apparent noncompetitive behavior with respect to peptide. However, the same experiments carried out at SAM concentrations near or below the K_m of SAM (0.3 ± 0.1 μM) (Table 1) resulted in a broadly linear increase in IC_{50} values more consistent

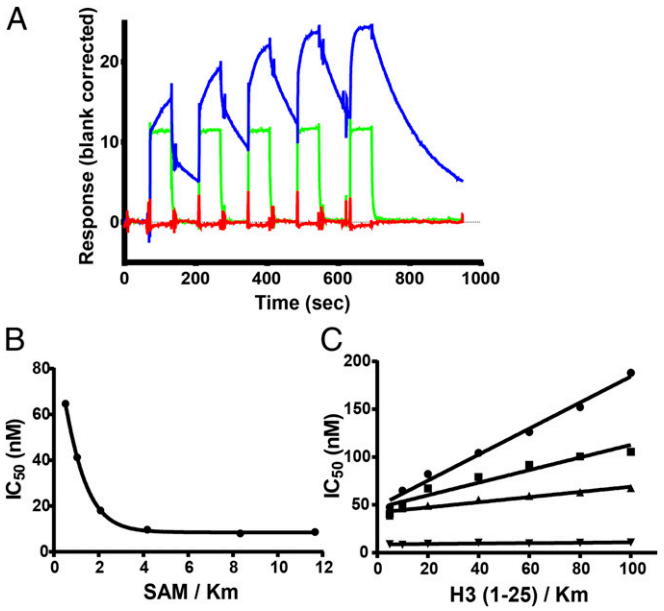

Fig. 3. (*R*)-PFI-2 is a SAM-dependent inhibitor of SETD7. (*A*) Biacore SPR sensorgram of (*R*)-PFI-2 and SAM binding to SETD7. Three single-cycle kinetics runs with five concentrations were performed. Five injections of 20 μM SAM show consistent binding with rapid on and off kinetics (green); 20 μM SAM is expected to be saturating as the K_D of SAM for SETD7 was determined to be 1.1 μM under these conditions. In the absence of SAM, a five-point dilution series of (*R*)-PFI-2 from 7.8 nM to 125 nM exhibited no binding to SETD7 (red). When the (*R*)-PFI-2 injections included 20 μM SAM, a visually biphasic binding curve was observed, reflecting fast SAM binding with subsequent slower (*R*)-PFI-2 binding (blue). At the highest (*R*)-PFI-2 concentration (rightmost blue curve), the dissociation curve was single phase whereas, at lower (*R*)-PFI-2 concentrations, the dissociation curves were biphasic. Under these latter conditions, SETD7 is essentially saturated with SAM, but the (*R*)-PFI-2 concentrations were not fully saturating and the protein is a mix of SAM-bound and SAM plus (*R*)-PFI-2 bound. This situation gives rise to two visibly different off rates, one for SAM alone and one for the combination of SAM plus (*R*)-PFI-2. A single-cycle kinetics methodology was used. The analysis was done in triplicate using a 1:1 kinetic fitting model and the data were processed separately and values were averaged. (*B*) IC_{50} values were determined for (*R*)-PFI-2 at varying concentrations of SAM, 5 μM peptide, and 20 nM enzyme. (*C*) IC_{50} values at varying concentrations of substrate H3(1–25) peptide and at SAM concentrations of 0.125 (●), 0.25 (■), 0.5 (▲), and 2 μM (▼) using 20 nM enzyme as described in *SI Appendix*.

with a competitive mode of inhibition with respect to peptide. This effect was most pronounced at the lowest SAM concentrations (Fig. 3*C*). These data are consistent with our structural observations that (*R*)-PFI-2 binds to the peptide-binding site but also interacts with the methyl group of SAM. Altogether, our data indicate that inhibition of SETD7 activity by (*R*)-PFI-2 is unlikely to be purely substrate-competitive in the classical sense; rather, it is complicated by the interaction of (*R*)-PFI-2 with SAM.

(*R*)-PFI-2 Binds SETD7 in Cells. (*R*)-PFI-2 has favorable physicochemical properties, including high aqueous solubility (285 μM), permeability (Russel–Ralph canine kidney cell = 6.48×10^{-6} cm/sec; $LogD_{7.4}$ = 2.3), and stability (*SI Appendix*, Fig. S4*A*), suggesting that it is an excellent tool for cellular studies of SETD7 catalytic function. (*R*)-PFI-2 did not affect the viability of four different cell lines treated with (*R*)-PFI-2 at below 50 μM (*SI Appendix*, Fig. S4*B*). Cellular thermal shift assay (CETSA) that measures ligand-induced stabilization of a target protein in cells showed a 4 °C increase in the apparent thermal stability of Flag-tagged SETD7 in HEK293 cells at 10 μM (*R*)-PFI-2, indicating that (*R*)-PFI-2 passed through the cell membrane and bound to and stabilized SETD7 (*SI Appendix*, Fig. S4 *C* and *D*). To confirm that (*R*)-PFI-2 binds to endogenous human SETD7 in cells, we used structure-guided molecular design to generate PFI-766 (Fig. 4*A*), a biotinylated variant of (*R*)-PFI-2 that retains the ability to bind and inhibit SETD7 (IC_{50} 110 ± 26 nM in our in vitro enzymatic assay). We used PFI-766 (Fig. 4*A*) immobilized on streptavidin beads to isolate endogenous SETD7 from lysates of MCF7 cells pretreated (for 1 h or 5 h) with increasing doses of (*R*)-PFI-2 (Fig. 4 *B* and *C*). The amount of SETD7 "pulled down" by the beads was largely competed off by both 1-h and 5-h pretreatment of live cells with 5μM (*R*)-PFI-2. Because the lysed material in these experiments was diluted by ∼15-fold, we estimate a cellular IC_{50} for binding of (*R*)-PFI-2 to endogenous SETD7 in the submicromolar range (i.e., 15-fold less than in the cell lysate). PFI-766 engagement of endogenous SETD7 was also confirmed by mass spectrometry that supported the high specificity of the compound for endogenous SETD7 (*SI Appendix*, Table S3). Taken together, these results demonstrate direct binding of endogenous SETD7 by (*R*)-PFI-2 in a cellular environment.

(*R*)-PFI-2–Dependent Inhibition of SETD7 Affects Yes-Associated Protein Localization and Phenocopies Setd7 Genetic Deletion. We have recently identified a role for SETD7 in Hippo pathway signaling in vitro and in vivo (31). The Hippo pathway is an evolutionarily conserved regulator of cellular proliferation, survival, and organ size (32). Activation of the Hippo pathway by cell–cell contact results in the phosphorylation and cytoplasmic retention of the transcriptional coactivator Yes-associated protein (YAP), resulting in decreased expression of YAP target genes such as *Areg*, *Cdc20*, *Ctgf*, *Cyr61*, and *Gli2*. In *Setd7*$^{-/-}$ murine embryonic fibroblasts (MEFs), cell–cell contact does not lead to YAP sequestration in the cytoplasm, resulting in increased levels of nuclear YAP and heightened expression of YAP target genes. Although direct methylation of Yap by SETD7 was not demonstrated, these effects were dependent on the methyltransferase activity of SETD7, as well as a putative methylation site (K494) of YAP (31), thus supporting a role for

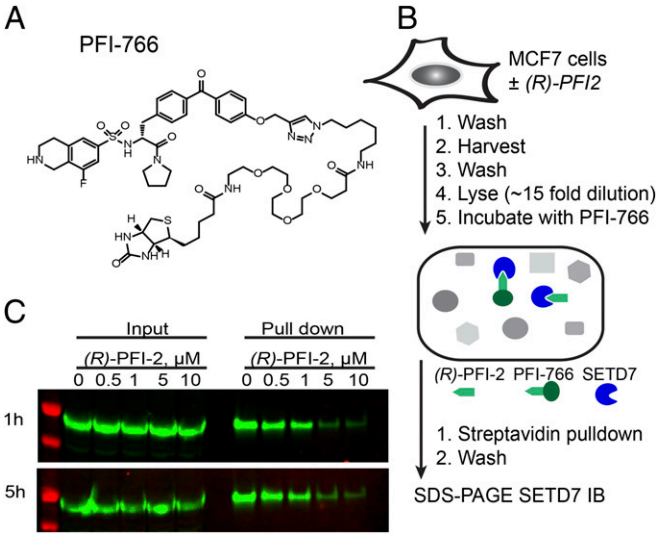

Fig. 4. (*R*)-PFI-2 binds to SETD7 in cells. (*A*) Structure of PFI-766. (*B*) Schematic of the experiment using PFI-766 to pull down endogenous SETD7. (*C*) PFI-766 pulls down endogenous SETD7 from washed MCF7 cells, and the amount of pulled-down material decreased in a dose-dependent manner in cells treated with increasing doses of (*R*)-PFI-2. The control lane of 0 (*R*)-PFI-2 indicates the solvent DMSO control. The gels shown are representative of at least three independent experiments.

a novel methylation-dependent checkpoint in activation of the Hippo pathway. Consistent with a role for the methyltransferase activity of SETD7 in regulating YAP localization, *Setd7*$^{+/+}$ MEFs grown to confluence in the presence of (*R*)-PFI-2, but not the less-active enantiomer, displayed increased nuclear localization of YAP as measured by immunofluorescence using two distinct antibodies (Fig. 5*A* and *SI Appendix*, Fig. S5 *A* and *B*), as well as increased expression of YAP-dependent genes *Ctgf*, *Gli2*, and *Cdc20* (Fig. 5*B* and *SI Appendix*, Fig. S5*C*). Similar to results in *Setd7*$^{-/-}$ MEFs, (*R*)-PFI-2–dependent inhibition of SETD7 activity had no effect on YAP localization at low cell density when Yap is primarily nuclear (Fig. 5*A*). (*R*)-PFI-2 had no effect in *Setd7*$^{-/-}$ MEFs, further supporting a SETD7-specific effect (Fig. 5 *A* and *B* and *SI Appendix*, Fig. S5*C*). Furthermore, when we transfected *Setd7*$^{-/-}$ MEFs with plasmids expressing either SETD7 or SETD7^{H252W}, we found that nuclear accumulation of YAP after (*R*)-PFI-2 treatment was inhibited by the H252W mutation (*SI Appendix*, Fig. S5*D*), consistent with the proposed interactions between (*R*)-PFI-2 and SETD7. Taken together, these results demonstrate that (*R*)-PFI-2, through direct interactions with SETD7, modulates YAP localization.

One of the key advantages of a pharmacological agent over genetic methods for studying gene/protein function is the ability to study temporal and dynamic processes in cells (24). We therefore sought to exploit (*R*)-PFI-2 to interrogate the mechanistic role of human SETD7 in cells in which the Hippo/YAP pathway was already activated. We treated confluent MCF7 cells with (*R*)-PFI-2 or (*S*)-PFI-2 for 2 h and examined the subcellular localization of YAP. Strikingly, treatment of high-density MCF7 cells with (*R*)-PFI-2 resulted in a dose-dependent increase of nuclear YAP (Fig. 5 *C–E*) and heightened expression of the YAP target genes *AREG* and *CYR61* (*SI Appendix*, Fig. S5*G*) whereas (*S*)-PFI-2 had no effect (*SI Appendix*, Fig. S5 *E* and *F*). These results indicate that YAP localization in confluent MCF7 cells is the net result of a dynamic process that requires constant SETD7 activity. In support of this concept, kinetic analysis showed that inhibition of SETD7 with (*R*)-PFI-2 led to increased YAP nuclear localization within 30 min of treatment (Fig. 5*F*), indicating that the effects of SETD7-dependent methylation can be rapidly reversed in cells through inhibition of the enzyme. Together, these results demonstrate SETD7-dependent cellular activity for (*R*)-PFI-2 and indicate that SETD7-dependent methylation is operating in a continuous and dynamic process to control the subcellular localization and function of YAP following activation of the Hippo pathway.

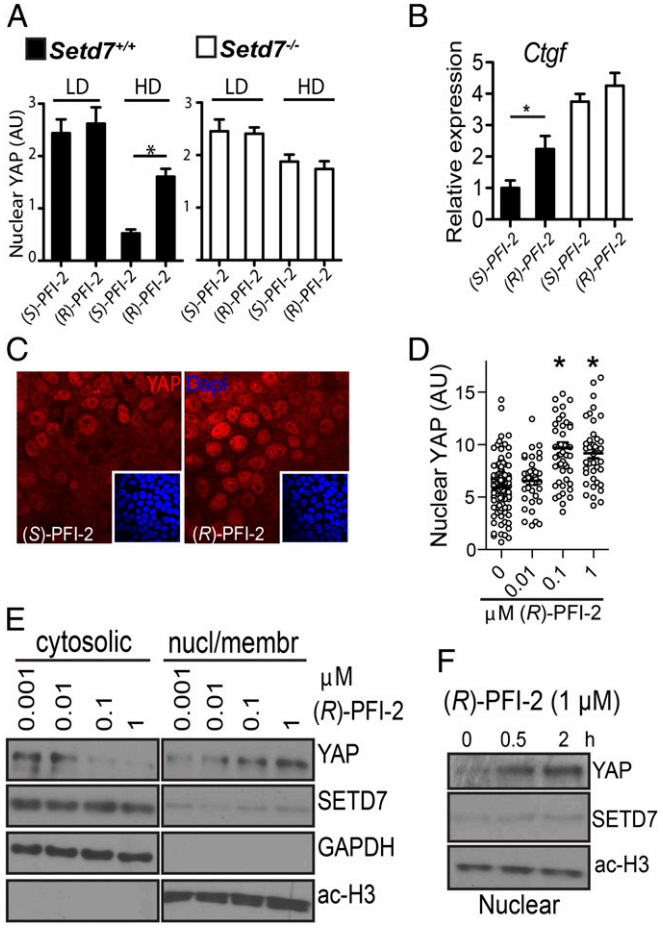

Fig. 5. Inhibition of Setd7 affects YAP in MEFs and MCF7 cells. (*A*) MEFs derived from *Setd7*$^{+/+}$ or *Setd7*$^{-/-}$ mice were grown at low density (LD) or high density (HD) in the presence of 10 μM (*S*)-PFI-2 or (*R*)-PFI-2. The amount of nuclear YAP was quantified from images as described in *SI Appendix*. Data from three experiments were pooled ($n > 30$; *$P < 0.001$). (*B*) (*R*)-PFI-2 treatment induces YAP target genes in high-density *Setd7*$^{+/+}$ MEF cultures. Relative expression is displayed as the expression levels of *Ctgf* after (*R*)-PFI-2 treatment over that with (*S*)-PFI-2 treatment prenormalized to the levels of *Actb* housekeeping gene ($n = 6$; *$P < 0.05$). (*C*) Confluent MCF7 cultures were treated with (*S*)-PFI-2 or (*R*)-PFI-2 for 2 h at 1 μM, and stained for the Hippo pathway transducer YAP (red) and DAPI (blue). Representative confocal images of equal magnification (150 × 150 μm) are shown. (*D*) The amount of nuclear YAP quantified from images in *C*. Data are from two pooled experiments ($n > 30$; *$P < 0.001$). (*E*) Confluent MCF7 cells were treated with the indicated concentrations of (*R*)-PFI-2 for 2 h and show a clear decrease in cytosolic YAP with simultaneous increase in nuclear YAP with increasing (*R*)-PFI-2. (*F*) Confluent MCF7 cultures were incubated with 1 μM (*R*)-PFI-2 for the indicated times. Western blots of nuclear extracts were probed for YAP, SETD7, and ac-H3.

Discussion

Increasing evidence implicates SETD7 as a regulator of nonhistone proteins, especially transcription factors and chromatin regulators, which in turn modulate gene expression patterns within specific signaling pathways. However, identification of distinct, widely replicated phenotypes associated with these SETD7 activities is still lacking. Studies identifying a role for SETD7 in a wide variety of signaling pathways [e.g., NF-κB (8, 16), p53 (5), STAT3 (15), and ER (13)] have all used knockdown/-out of the entire protein or overexpression in transformed cell lines, which may obscure or exaggerate subtle regulatory mechanisms. Under homeostatic conditions, *Setd7*$^{-/-}$ mice fail to support a role in these previously identified pathways (17, 18, 31). However, it is possible that, under specific conditions of stress or inflammation, a more dramatic role for *Setd7* in these pathways may emerge. Thus, SETD7-dependent methylation may yet prove to be an important regulatory mechanism and a novel therapeutic target in diseases associated with these important signaling pathways.

Here, we report a chemical tool kit for the investigation of the molecular and functional role of endogenous SETD7 in cellular signaling and gene expression. (*R*)-PFI-2 is a potent and selective inhibitor of SETD7's catalytic activity. Its enantiomer, (*S*)-PFI-2, is 500-fold less active and serves as a structurally similar negative control molecule for comparison. PFI-766 is an analog of (*R*)-PFI-2 that retains strong binding and inhibition and can be derivatized for chemoproteomics and other cellular studies (23). We used these reagents to demonstrate the specificity of the cellular response, target engagement in cells, and the pharmacological modulation of SETD7 in Hippo signaling in MEFs and MCF7 cells. Our results indicate that SETD7-dependent regulation of YAP localization is a rapid and dynamic process. Of note, it remains unresolved whether these methylation-dependent events are due to direct methylation of the YAP protein itself, or whether additional substrates are involved. Thus, given the many

potential pathways in which SETD7 has been implicated in human cell signaling (10, 12), (*R*)-PFI-2 and related compounds will be valuable tools for the community to better understand SETD7 biology.

Finally, our combined structural, biophysical, and enzymatic analyses showed that (*R*)-PFI-2 has a distinctive cofactor-dependent mode of action, combined with a likely substrate-competitive contribution. As such, (*R*)-PFI-2 is the third recent example of highly selective inhibitors that bind in the substrate peptide-binding groove of SET domain methyltransferases [in addition to methyltransferase G9a/GLP (33) and SMYD2 inhibitors (34)], suggesting that targeting the peptide-binding groove may be a general strategy for other human PKMTs, many of which are attractive therapeutic targets (25, 35).

Materials and Methods

Recombinant human SETD7 (residues 1–366) and SET domain only (residues 109–366) were expressed in *Escherichia coli* and purified to homogeneity. Methyltransferase activity of SETD7(1-366) was assayed using a scintillation proximity assay monitoring the incorporation of the tritium-labeled methyl group of ^{3}H-SAM into a peptide substrate corresponding to histone H3 residues 1–25 at 2 μM SAM and 2 μM H3(1–25) and 2 nM enzyme (Fig. 1).

SETD7(109–366) crystallized with (*R*)-PFI-2 in 23% PEG 3500, 0.1 M lithium sulfate, and 0.1 M BisTris (pH 6.5). Further details, along with protein purification, enzymatic mechanism of action studies, biophysical binding measurements, and chemistry methods, are described in *SI Appendix*.

Cellular assays of YAP localization were performed in MEFs at both low and high density, and confluent MCF7 cells were treated with the indicated concentrations of (*R*)-PFI-2 or (*S*)-PFI-2. Nuclear YAP was quantified using ImageJ software using two different YAP antibodies. Further details of image analysis and statistics, along with methods for RNA isolation, Western blots of cytosolic and nuclear protein extracts, and RT-PCR, are described in *SI Appendix*.

ACKNOWLEDGMENTS. We thank members of the M.V. laboratory and the Pfizer high-throughput screen (HTS) team for assays and HTS. (*R*)-PFI-2 is now commercially available from Tocris. Small amounts of (*S*)-PFI-2 or PFI-766 are available for research purposes upon request from Structural Genomics Consortium (SGC). The SGC is a registered charity (no. 1097737) that receives funds from AbbVie, Boehringer Ingelheim, the Canada Foundation for Innovation (CFI), the Canadian Institutes of Health Research (CIHR), Genome Canada, Ontario Genomics Institute Grant OGI-055, GlaxoSmithKline, Janssen, Lilly Canada, the Novartis Research Foundation, the Ontario Ministry of Economic Development and Innovation, Pfizer, Takeda, and Wellcome Trust Grant 092809/Z/10/Z. Use of the Advanced Photon Source was supported by US Department of Energy Contract DE-AC02-06CH11357. This work was supported by CIHR Grants MOP-123322 (to A.-C.G.) and MSH-95368, MOP-89773, and MOP-106623 (to C.Z.) and a CFI grant (to C.Z.). C.Z. is a Michael Smith Foundation for Health Research Career Investigator. M.J.O. is the recipient of CIHR/Canadian Association of Gastroenterology/Janssen Inc. and Michael Smith Foundation for Health Research postdoctoral fellowships. C.H.A. holds a Canada Research Chair in Structural Genomics.

1. Nishioka K, et al. (2002) Set9, a novel histone H3 methyltransferase that facilitates transcription by precluding histone tail modifications required for heterochromatin formation. *Genes Dev* 16(4):479–489.
2. Wang H, et al. (2001) Purification and functional characterization of a histone H3-lysine 4-specific methyltransferase. *Mol Cell* 8(6):1207–1217.
3. Calnan DR, et al. (2012) Methylation by Set9 modulates FoxO3 stability and transcriptional activity. *Aging (Albany, NY)* 4(7):462–479.
4. Carr SM, Munro S, Kessler B, Oppermann U, La Thangue NB (2011) Interplay between lysine methylation and Cdk phosphorylation in growth control by the retinoblastoma protein. *EMBO J* 30(2):317–327.
5. Chuikov S, et al. (2004) Regulation of p53 activity through lysine methylation. *Nature* 432(7015):353–360.
6. Deering TG, Ogihara T, Trace AP, Maier B, Mirmira RG (2009) Methyltransferase Set7/9 maintains transcription and euchromatin structure at islet-enriched genes. *Diabetes* 58(1):185–193.
7. Dhayalan A, Kudithipudi S, Rathert P, Jeltsch A (2011) Specificity analysis-based identification of new methylation targets of the SET7/9 protein lysine methyltransferase. *Chem Biol* 18(1):111–120.
8. Ea CK, Baltimore D (2009) Regulation of NF-kappaB activity through lysine monomethylation of p65. *Proc Natl Acad Sci USA* 106(45):18972–18977.
9. Estève PO, et al. (2009) Regulation of DNMT1 stability through SET7-mediated lysine methylation in mammalian cells. *Proc Natl Acad Sci USA* 106(13):5076–5081.
10. Keating ST, El-Osta A (2013) Transcriptional regulation by the Set7 lysine methyltransferase. *Epigenetics* 8(4):361–372.
11. Kouskouti A, Scheer E, Staub A, Tora L, Talianidis I (2004) Gene-specific modulation of TAF10 function by SET9-mediated methylation. *Mol Cell* 14(2):175–182.
12. Pagans S, et al. (2010) The cellular lysine methyltransferase Set7/9-KMT7 binds HIV-1 TAR RNA, monomethylates the viral transactivator Tat, and enhances HIV transcription. *Cell Host Microbe* 7(3):234–244.
13. Subramanian K, et al. (2008) Regulation of estrogen receptor alpha by the SET7 lysine methyltransferase. *Mol Cell* 30(3):336–347.
14. Wang J, et al. (2009) The lysine demethylase LSD1 (KDM1) is required for maintenance of global DNA methylation. *Nat Genet* 41(1):125–129.
15. Yang J, et al. (2010) Reversible methylation of promoter-bound STAT3 by histone-modifying enzymes. *Proc Natl Acad Sci USA* 107(50):21499–21504.
16. Yang XD, et al. (2009) Negative regulation of NF-kappaB action by Set9-mediated lysine methylation of the RelA subunit. *EMBO J* 28(8):1055–1066.
17. Campaner S, et al. (2011) The methyltransferase Set7/9 (Setd7) is dispensable for the p53-mediated DNA damage response in vivo. *Mol Cell* 43(4):681–688.
18. Lehnertz B, et al. (2011) p53-dependent transcription and tumor suppression are not affected in Set7/9-deficient mice. *Mol Cell* 43(4):673–680.
19. Schapira M (2011) Structural chemistry of human SET domain protein methyltransferases. *Curr Chem Genomics* 5(Suppl 1):85–94.
20. Li Y, et al. (2008) Role of the histone H3 lysine 4 methyltransferase, SET7/9, in the regulation of NF-kappaB-dependent inflammatory genes: Relevance to diabetes and inflammation. *J Biol Chem* 283(39):26771–26781.
21. Okabe J, et al. (2012) Distinguishing hyperglycemic changes by Set7 in vascular endothelial cells. *Circ Res* 110(8):1067–1076.
22. Garbino A, et al. (2009) Molecular evolution of the junctophilin gene family. *Physiol Genomics* 37(3):175–186.
23. Bunnage ME, Chekler EL, Jones LH (2013) Target validation using chemical probes. *Nat Chem Biol* 9(4):195–199.
24. Frye SV (2010) The art of the chemical probe. *Nat Chem Biol* 6(3):159–161.
25. Arrowsmith CH, Bountra C, Fish PV, Lee K, Schapira M (2012) Epigenetic protein families: A new frontier for drug discovery. *Nat Rev Drug Discov* 11(5):384–400.
26. Copeland RA, et al. (1995) Recombinant human dihydroorotate dehydrogenase: Expression, purification, and characterization of a catalytically functional truncated enzyme. *Arch Biochem Biophys* 323(1):79–86.
27. Ribeiro C, Esteves da Silva JC (2008) Kinetics of inhibition of firefly luciferase by oxyluciferin and dehydroluciferyl-adenylate. *Photochem Photobiol Sci* 7(9):1085–1090.
28. Xiao B, et al. (2003) Structure and catalytic mechanism of the human histone methyltransferase SET7/9. *Nature* 421(6923):652–656.
29. Ibáñez G, McBean JL, Astudillo YM, Luo M (2010) An enzyme-coupled ultrasensitive luminescence assay for protein methyltransferases. *Anal Biochem* 401(2):203–210.
30. Copeland RA (2013) *Evaluation of Enzyme Inhibitors in Drug Discovery: A Guide for Medicinal Chemists and Pharmacologists* (Wiley, Hoboken, NJ).
31. Oudhoff MJ, et al. (2013) Control of the hippo pathway by Set7-dependent methylation of Yap. *Dev Cell* 26(2):188–194.
32. Pan D (2010) The hippo signaling pathway in development and cancer. *Dev Cell* 19(4):491–505.
33. Vedadi M, et al. (2011) A chemical probe selectively inhibits G9a and GLP methyltransferase activity in cells. *Nat Chem Biol* 7(8):566–574.
34. Ferguson AD, et al. (2011) Structural basis of substrate methylation and inhibition of SMYD2. *Structure* 19(9):1262–1273.
35. Wigle TJ, Copeland RA (2013) Drugging the human methylome: An emerging modality for reversible control of aberrant gene transcription. *Curr Opin Chem Biol* 17(3):369–378.